



# Correlation analysis between the jet exhaust velocity field and microphone-array acoustic measurements for a turbo-fan engine

Alessandro Bassetti,<sup>\*</sup>Tobias Berkefeld,<sup>†</sup>Andreas Schröder,<sup>‡</sup>Henri Siller,<sup>§</sup>and Björn Wrede<sup>¶</sup>

*German Aerospace Center*

Simultaneous flow and acoustic measurements have been acquired for an aircraft, during ground operation. Measurements of velocity field data with stereoscopic particle image velocimetry (SPIV) on the engine-exhaust jet are correlated with the acoustic-pressure signals of a 120 microphone linear array. The turbulent velocity and the applied-stress components of the Lighthill- and Lilley-analogy source terms in the SPIV region are correlated with the microphone array. Convection effects on the propagating sound waves are neglected in the present study. The self-noise term in the Lighthill quadrupole, shows a hot spot for the correlation in the by-pass to ambient shear layer. This high correlation region is clearly visible in one of the analysed test points only, while in general a poor statistical convergence seems to affect the test-source correlation.

## Nomenclature

$C_i$	Correlation of the source model $s_i$ at a pixel of the SPIV image with the pressure signals measured in the whole array.
$N_i$	Normalization factor of the source model $s_i$ .
$N_{MIC}$	Number of microphones in the linear array.
$N_{PIV}$	Number of PIV images acquired for a given test point.
$\mathbf{r}$	Vector connecting the source position to the observer position.
$\mathbf{u}$	Fluctuating velocity.
$c_0$	Speed of sound.
$r_m$	Distance between a given pixel in the SPIV image and the microphone $m$ in the array.
$s_1$	Projection of the fluctuating velocity on the source-observer direction.
$s_2$	Shear noise term of the Lighthill quadrupole projected on the source-observer direction.
$s_3$	Self noise term of the Lighthill quadrupole projected on the source-observer direction.
$s_4$	Projection of the Lilley-analogy applied-stress source on the source-observer direction.

## I. Introduction

Within the SAMURAI project, DLR performed an experimental study of the aerodynamic and acoustic properties of an engine-exhaust jet during ground operation in the noise protection hangar of Hamburg airport.

<sup>\*</sup>Institute of Propulsion Technology, Engine Acoustics, Berlin; email: alessandro.bassetti@dlr.de

<sup>†</sup>Institute of Aerodynamics and Flow Technology, Experimental Methods, Göttingen

<sup>‡</sup>Institute of Aerodynamics and Flow Technology, Experimental Methods, Göttingen

<sup>§</sup>Institute of Propulsion Technology, Engine Acoustics, Berlin

<sup>¶</sup>Institute of Aerodynamics and Flow Technology, Experimental Methods, Göttingen

The experiments were performed in September 2013 with the DLR research aircraft ATRA parked, with the brakes on, while its IAE V2527 turbo-fan engines operated at different static speed settings. A large data base of aerodynamic and acoustic data has been acquired using stereoscopic particle-image velocimetry (SPIV) and a line array of 120 microphones. The microphones were placed on the ground, parallel to the jet axis. The present study is centered on the correlation between the SPIV velocity field data and the acoustic pressure signals of the array microphones. It is based on the data acquired at the maximum-continuous-thrust (MCT) operating condition of the aircraft engine. Three runs are examined: the number 40, 41 and 42, in the Samurai test matrix. Further information regarding the SPIV on the jet exhaust is reported by Schröder.<sup>1</sup> Measurements taken with the full line array (the present study only uses the rear-arc microphones) and the corresponding acoustic data are described in Ref. [2]. Since the publication of the pioneering paper by Lighthill<sup>3</sup> in 1952, acoustic analogies have been used to associate the variables that characterize the state of a given aerodynamic field in the convective region with its acoustic emission in the far field. In a generalized acoustic-analogy approach, a linear differential equation is obtained by rearranging the continuum thermo-mechanics equations, regarding the non-linear terms as source terms. Different acoustic analogies present different analytical expressions for the source terms. In the present work, a first evaluation is presented on how different combinations of the velocity components in the PIV investigation region correlate with the sound field recorded by a line array of microphones. Specifically the applied-stress components of the Lighthill<sup>3</sup> and the Lilley<sup>4</sup> analogies are considered.

## II. SPIV and acoustic-array measurement for the exhaust jet

The SPIV and the acoustic-array data were acquired simultaneously, but on separate systems. The PIV data have been acquired over a period of 90 s. The SPIV investigation region is located in the lower part of the exhaust-jet, downstream of the nozzle exit, see schematic in Figure 1. It is a two-dimensional region of the vertical plane which includes the engine axis. The PIV data sets consists of about 2000 instantaneous, 3-component velocity fields. Because the acquisition time of the microphone array acquisition system was limited to 30 s per data set, 3 separate records were recorded for each test case with a short gap of about two seconds between two successive recordings. The synchronization between the two measurements was ensured by recording an IRIG-B time code and the trigger signal of the SPIV images together with the microphone signals.

## III. Test source models and their correlations to the array measurements

The SPIV data are used to construct models for the instantaneous source field that can be correlated with the microphone time records. The following source models have been used for the correlation analysis.

1. The fluctuating-velocity field in the observer direction:  $s_1 = u'_r$
2. The shear- and self-noise terms of the Proudman-form Lighthill tensor at constant density and in the observer direction:  $s_2 = \langle u_r \rangle u'_r$  and  $s_3 = u'_r u'_r$ .
3. The Lilley-analogy applied stress term, with observer-direction fluctuating term given as:  $s_4 = (u'_i u'_j - \langle u'_i u'_j \rangle) r_i r_j$ , where repeated indices indicate a sum across the spatial coordinates.

The fluctuating velocity  $\mathbf{u}'$  is evaluated by subtracting the mean velocity  $\langle \mathbf{u} \rangle$  from the instantaneous velocity  $\mathbf{u}$ . The operator  $\langle \rangle$  indicates averaging. The source–observer vector is indicated by  $\mathbf{r}$ . The subscripts  $i$ ,  $j$  and  $k$  indicate a vector component along Cartesian coordinate axes. The subscript  $r$  indicates the projection along the source–observer direction. Note that in the present study we do not consider convection effects on the sound propagation. The vector  $\mathbf{r}$  is then defined as the difference between the fixed-frame positions of observer (i. e. a microphone of our array) and source (i. e. a pixel in the PIV frame). The source terms, after projection on  $\mathbf{r}$ , are given by a scalar. For each source  $s_i$  and each microphone, each PIV image can be transformed to have an instantaneous volumetric-source-strength field. By considering the effect on each microphone of the modelled source strength, one can proceed to average across the whole array and the whole

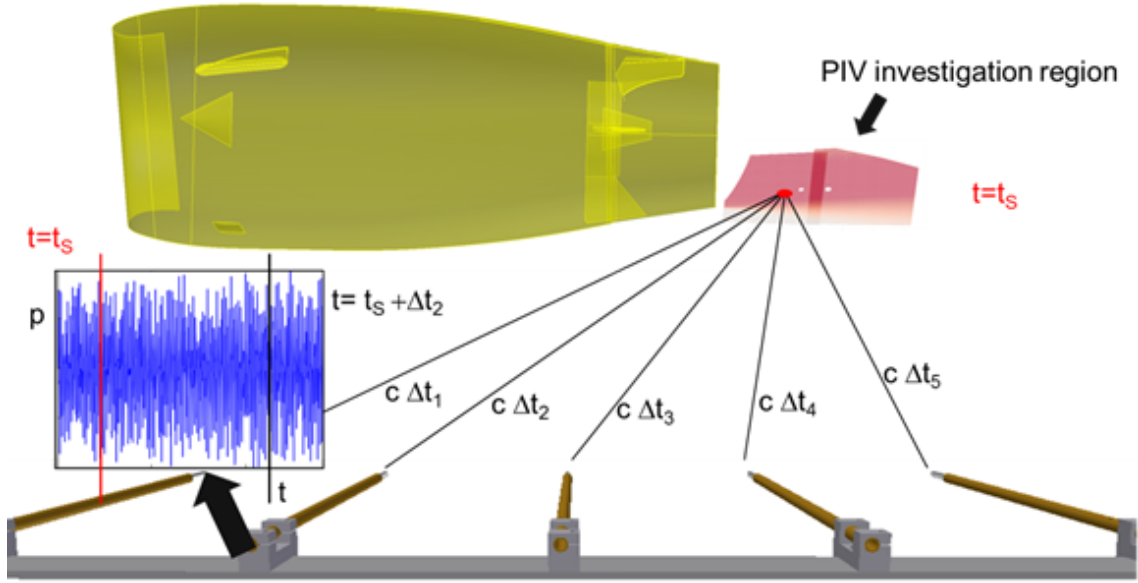


Figure 1. Position of the SPIV investigation region with respect to the IAEV2527 engine: the investigation region is a vertical slice, placed on a plane containing the engine axis. It includes the initial region of the jet exhaust shear layer, on the ground side of the jet. Two partially overlapping regions indicate the parts of the acquired fields, where the particle image data resulted in estimations of the instantaneous velocity field.

set of PIV images, in order to get the fields in Figure 2. In Figure 2 we report results for the Run 40. In Figures 2 to 11, the horizontal and vertical axes of the diagrams report respectively axial and vertical positions (in meters and with respect to the center of the engine exhaust cone) of the PIV investigation region. The result for the fluctuating Reynolds stress  $s_4$  is reported in Figure 3 for the test runs 40, 41 and 42 of the Samurai test matrix. The correlation function associated with the test source models is evaluated for each pixel in the PIV investigation region and for each microphone in the measurement array. Each pixel is connected to a given microphone  $m$  with its own source-observer vector  $\mathbf{r}_m$ . A pixel to microphone propagation time  $\Delta t$  is determined, assuming uniform speed of sound  $c$ . For the source models at each pixel, the correlation with the array signal is constructed by adding up the following contributions for the  $N_{PIV}$  SPIV images and for the  $N_{MIC}$  array microphones.

$$C_k = \frac{1}{N_{PIV} N_{MIC}} \sum_{i=1}^{N_{PIV}} \frac{1}{r_m} \sum_{m=1}^{N_{MIC}} s_k(t_i) p'(t_i + r_m/c) \quad (1)$$

The resulting correlation functions  $C_k$ , normalized by the surface-averaged RMS values of the given source field (the square root of the fields in Figure 2 is averaged across the PIV field to obtain the normalization factors for run 40), are the principal result of the present study. They are first presented in Figure 4 for the test sources  $s_1$  to  $s_4$  and the speed of sound of 337 m/s, corresponding to temperature records at Hamburg Airport, at the time of the measurement. The comparison in Figure 4 suggests that the statistical convergence is far to be reached (all results show positive-negative patterns and no clear hot spots). In Figure 4 it is also shown that the fluctuating velocity  $s_1$  assumes large correlation values also in the region outside the jet. This seems to suggest a poor performance of the source model  $s_1$  in capturing the source mechanisms of turbulent mixing noise. In the following, we restrict our analysis to the test models  $s_2$ ,  $s_3$  and  $s_4$ .

In Figures 5 to 7, we present the normalized correlation field for the terms,  $s_2$ ,  $s_3$  and  $s_4$ , at varying test point. Figure 6 (c) indicates that in run 42, possibly due to improved seeding conditions, we can observe a hot spot on the by-pass to ambient shear layer. The hot spot is especially visible for the source model  $s_3$  and also  $s_4$  seems to increase its correlation. A test of the sensitivity of the source-correlation distribution to changing speed of sound is presented in Figures 8 and 9, for the terms  $s_3$  and  $s_4$  and in run 40. The same test for run 42 can be seen in Figures 10 and 11. Changing the speed of sound in our transmission model seems not to affect

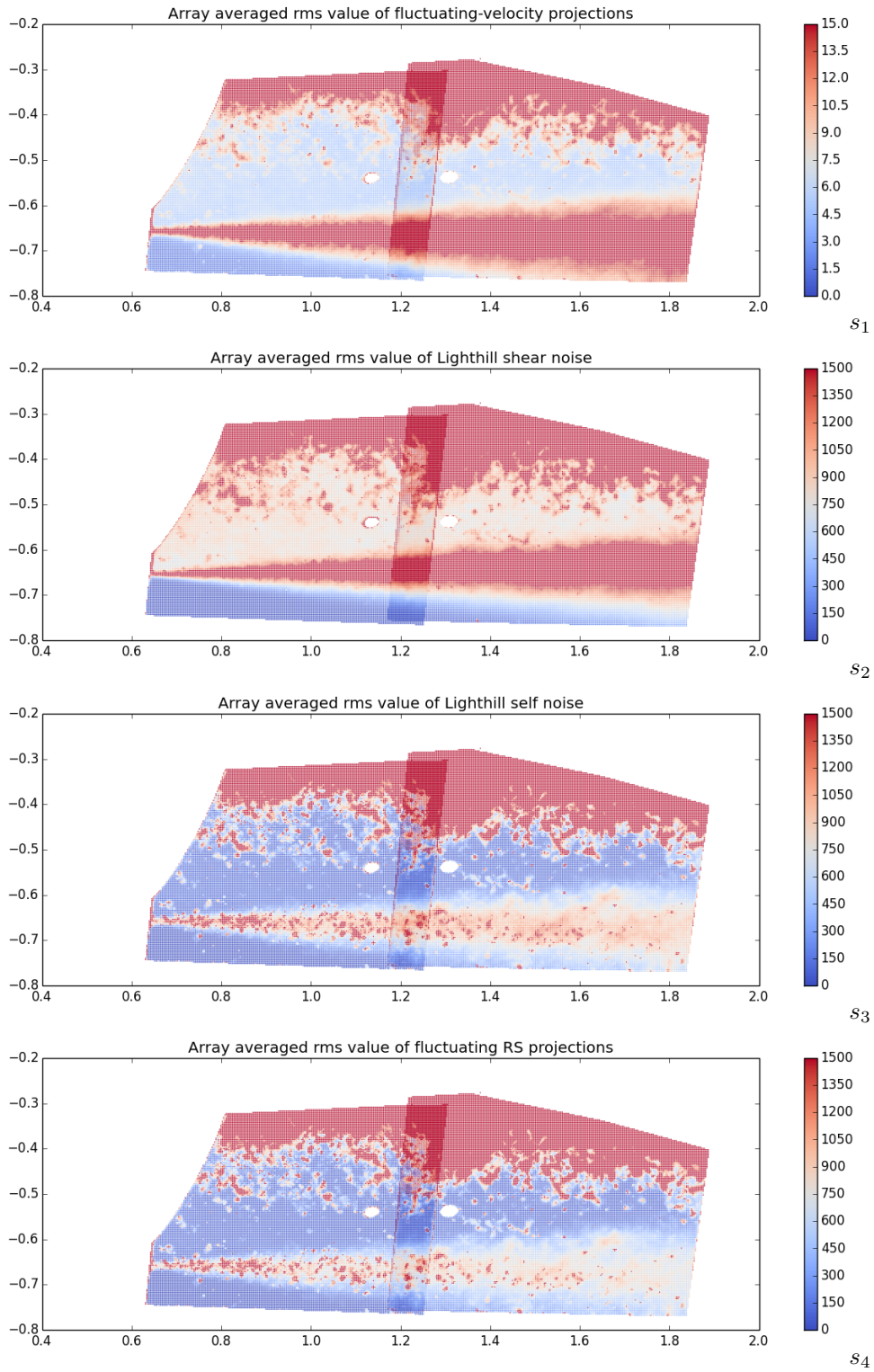
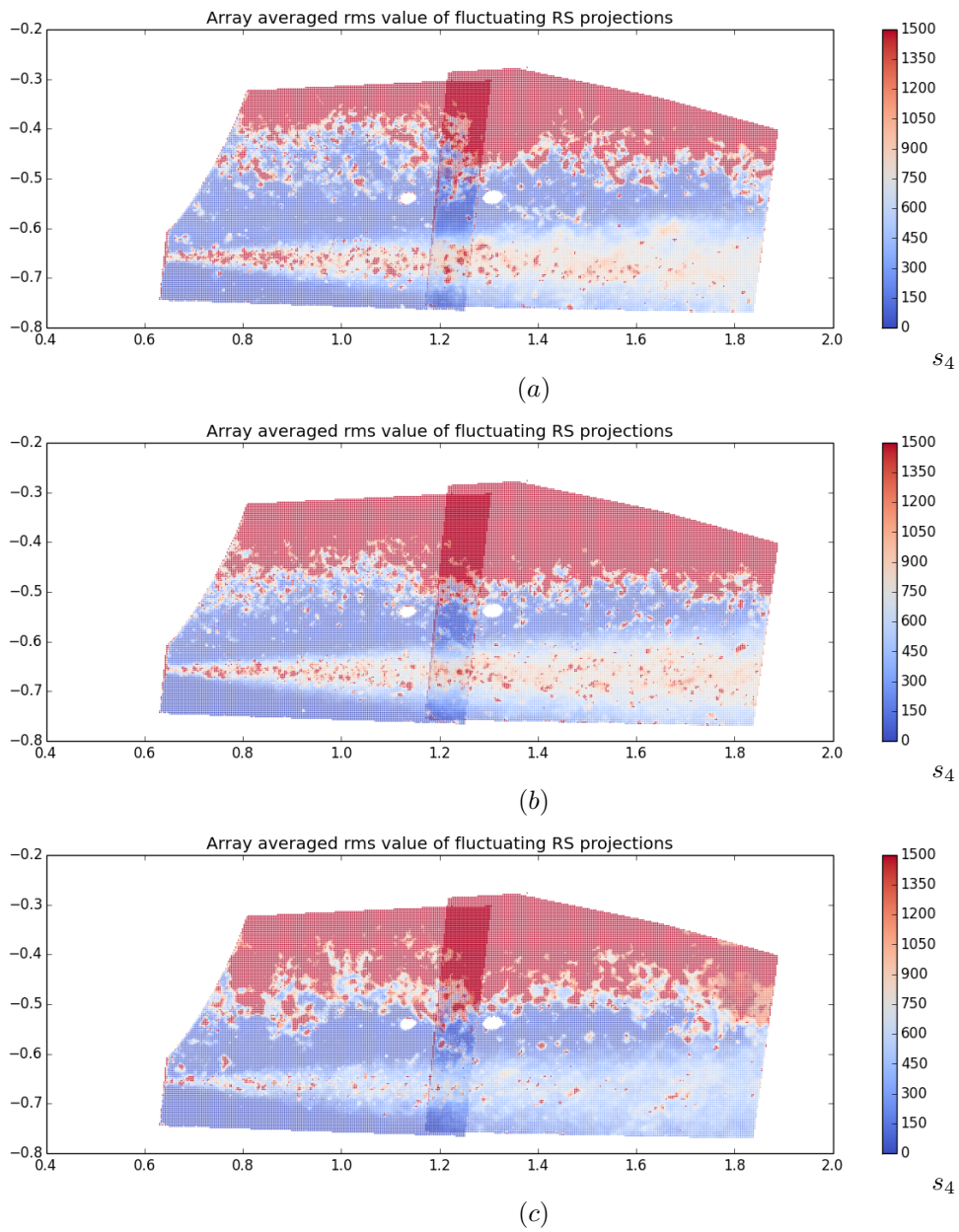


Figure 2. Average (across the whole array and the whole set of PIV images) of the RMS value of the source fields  $s_j$ , for the run 40.



**Figure 3.** Average (across the whole array and the whole set of PIV images) of the RMS value of the source field  $s_4$ , for the runs 40 (a), 41 (b) and 42 (c) of the Samurai test matrix.

the correlation patterns. A more accurate analysis is required in order to assess variation in the correlation magnitude.

## IV. Conclusions and Outlook

We performed a correlation analysis between PIV images and microphone-array records acquired during 3 test points. In the 3 test points, the aircraft engines were at maximum continuous thrust. The analysis included 4 test source models derivable from the velocity field of the PIV measurements. The analysis did not include convection effects on the sound propagation. The test source model  $s_3$ , representing the self-noise term in the Lighthill quadrupole, shows a hot spot for the correlation in the by-pass to ambient shear layer. This high correlation region is clearly visible in one of the analysed test points only, while in general a poor statistical convergence seems to affect the test-source correlation with the microphone array records.

Introducing a model for the sound convection seems a necessary step, especially if one wants to focus in the bypass to core region of the PIV images. Longer observation times and the combination of the results for more runs are the other steps which should improve the statistical convergence of the present analysis.

## References

- <sup>1</sup>Schröder, A., Geisler, R., Schanz, D., Wrede, B., and Agocs, J., “Flow field investigations in the free bypass jet flow of a V2527 engine at Ground Operation using SPIV,” Aiaa paper 2016–0108, Jan. 2016.
- <sup>2</sup>Siller, H., Bassetti, A., and Funke, S., “SAMURAI - jet noise source analysis of a V2500 engine,” Aiaa paper 2016–0110, Jan. 2016.
- <sup>3</sup>Lighthill, M. J., “On sound generated aerodynamically. I. General theory,” *Proceedings of the Royal Society of London. Series A, Mathematical and Physical Sciences*, Vol. 211, No. 1107, 1952, pp. 564–587.
- <sup>4</sup>Lilley, G. M., “Generation of sound in a mixing region,” *The Generation and Radiation of Supersonic Jet Noise — Volume IV — Theory of Turbulence Generated Jet Noise, Noise Radiation from Upstream Sources, and Combustion Noise*, Vol. 4, Air Force Aero Propulsion Laboratory, 1972, pp. 1–84.

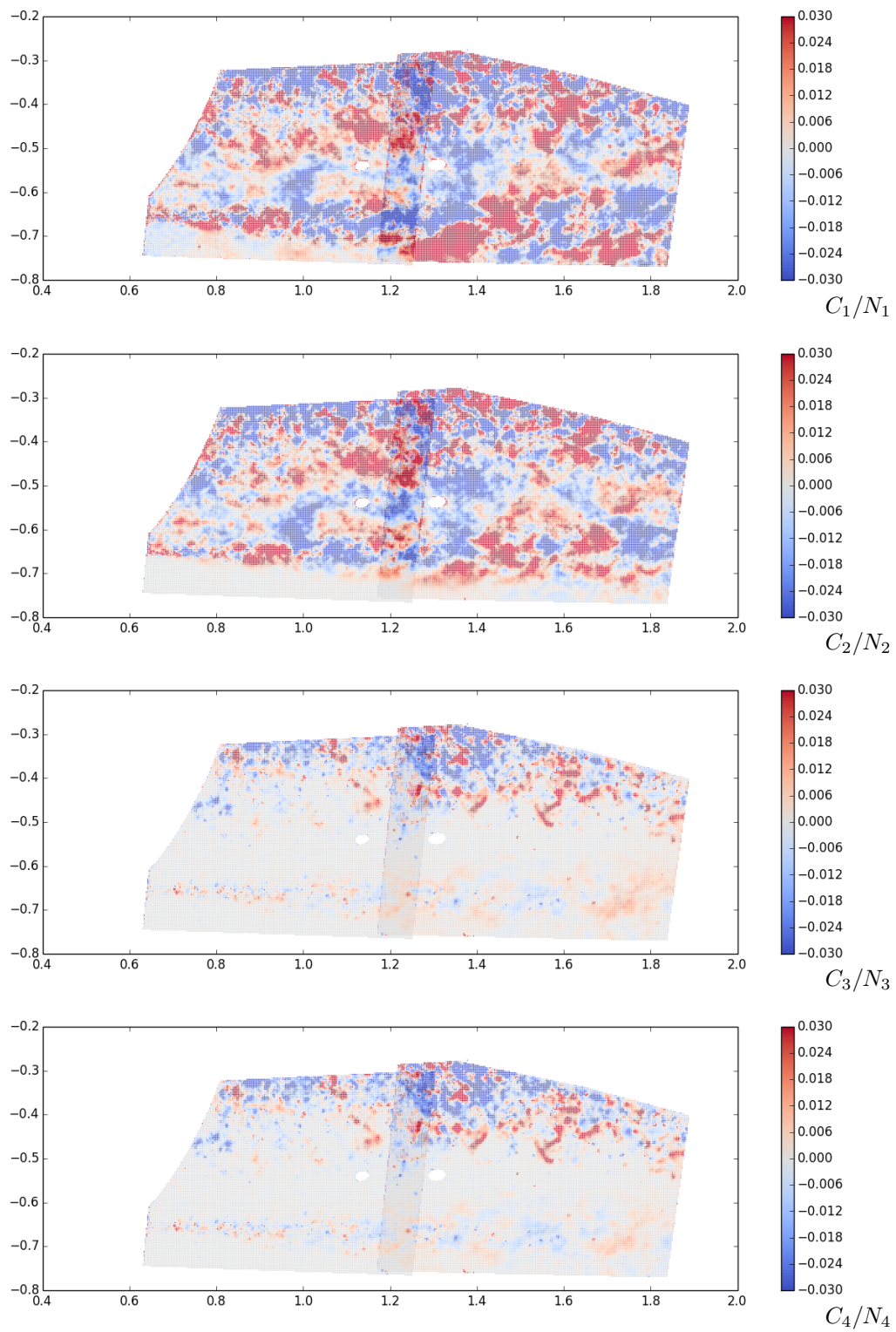


**Figure 4.** Normalized  $C_k$ , equation 1, for the test point 40 and assuming  $c=337$  m/s.

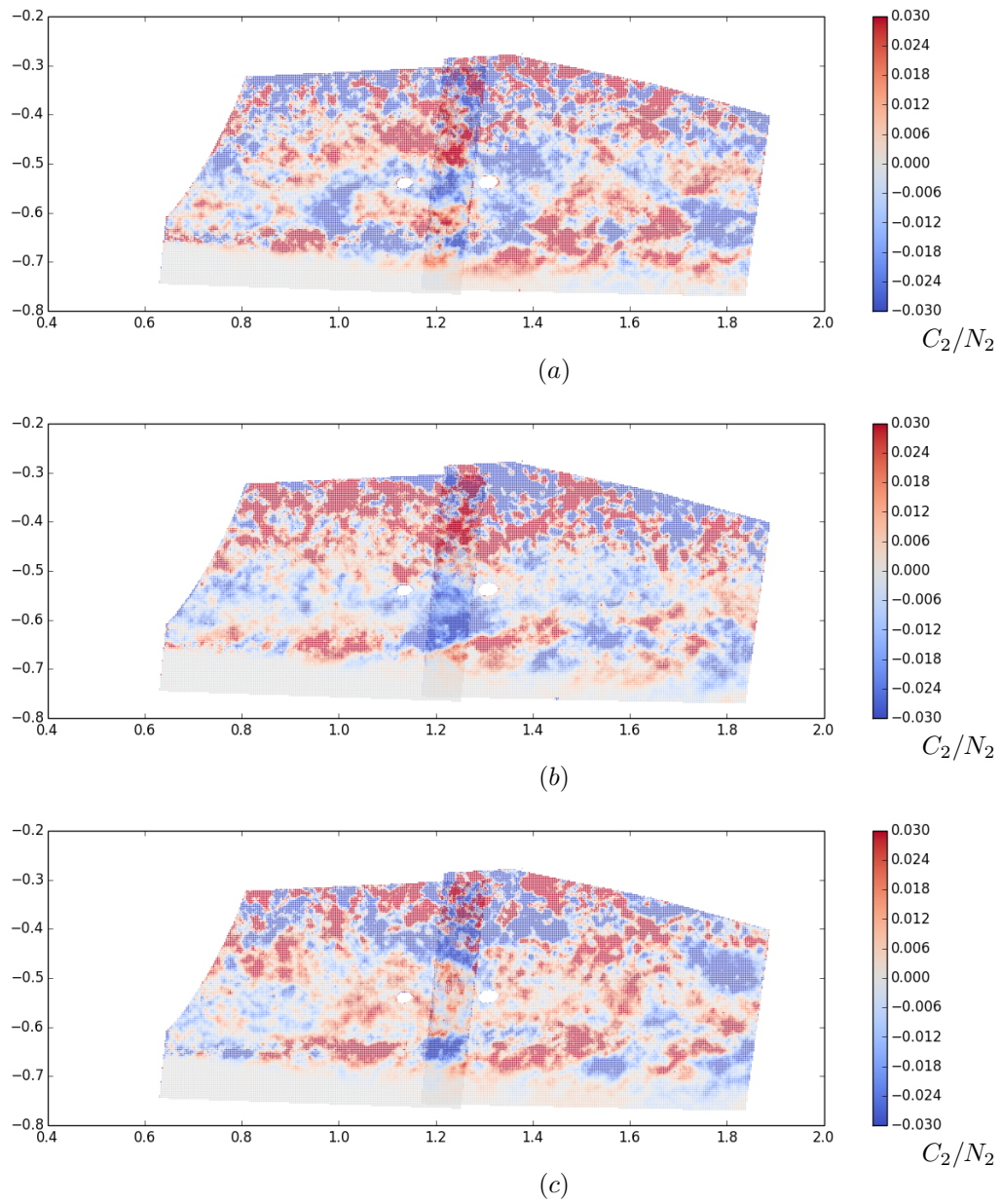


Figure 5. Normalized  $C_2$  for the test points 40 (a), 41 (b) and 42 (c), assuming  $c=337$  m/s.

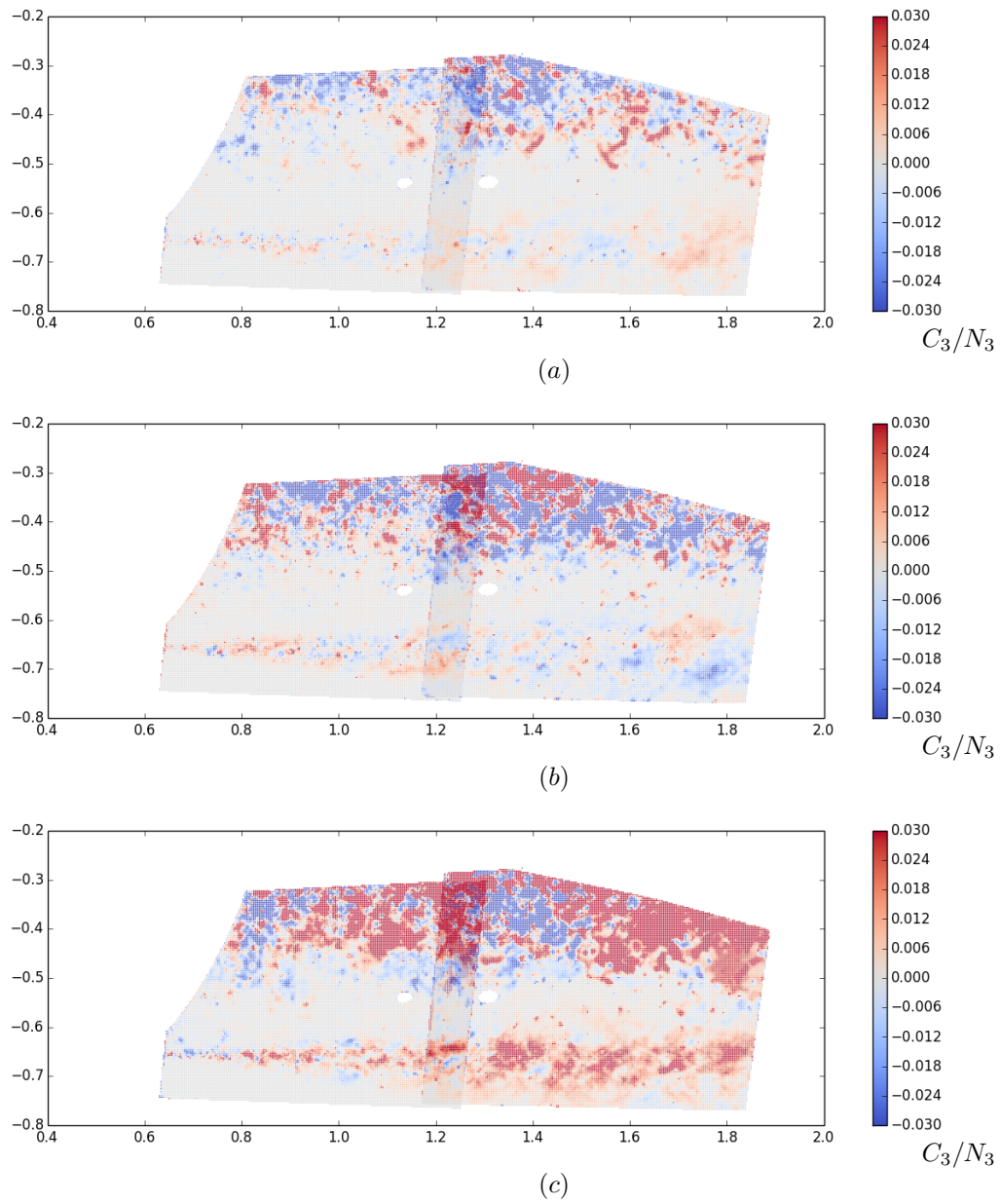


Figure 6. Normalized  $C_3$  for the test points 40 (a), 41 (b) and 42 (c), assuming  $c=337$  m/s.

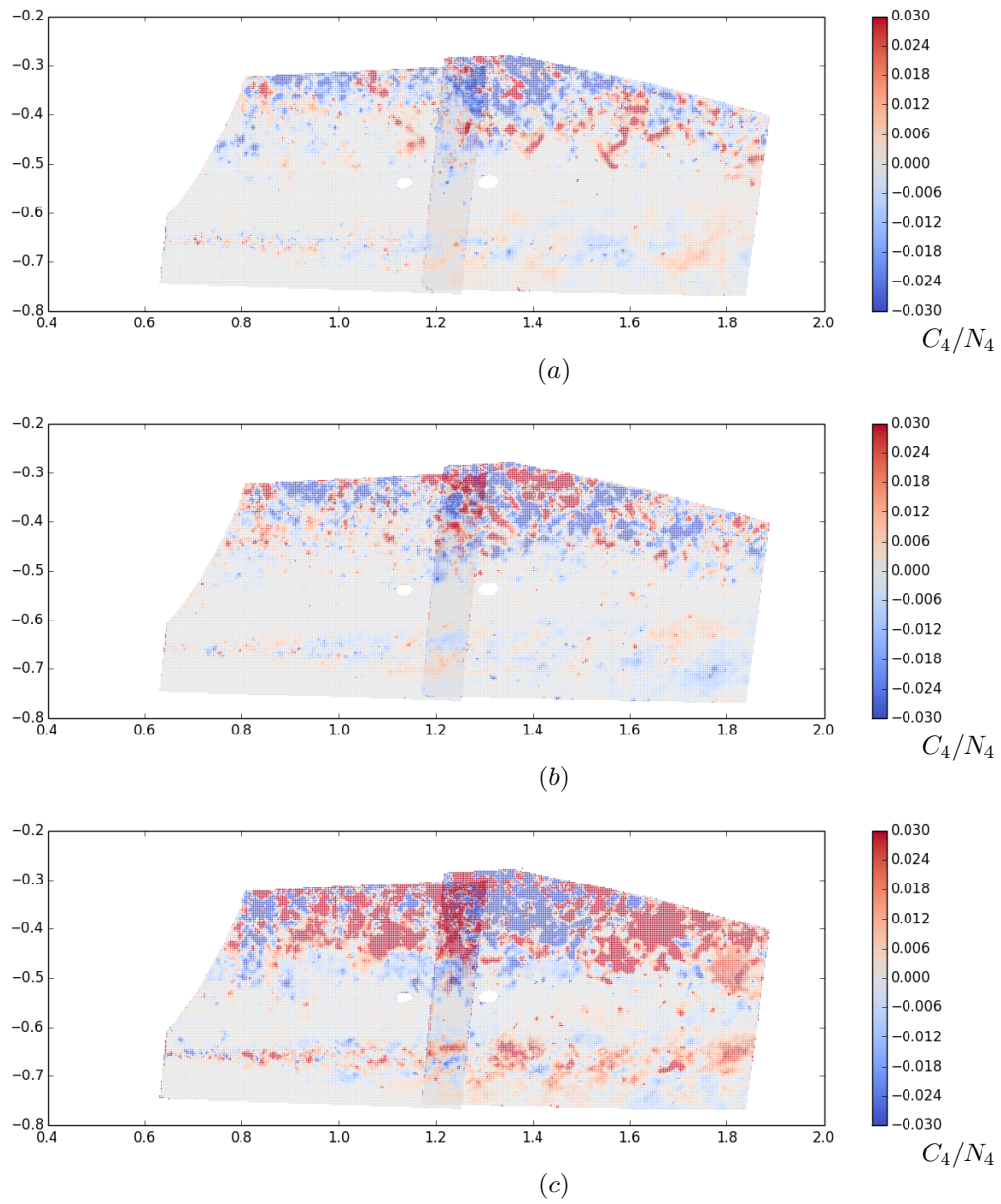


Figure 7. Normalized  $C_4$  for the test points 40 (a), 41 (b) and 42 (c), assuming  $c=337$  m/s.

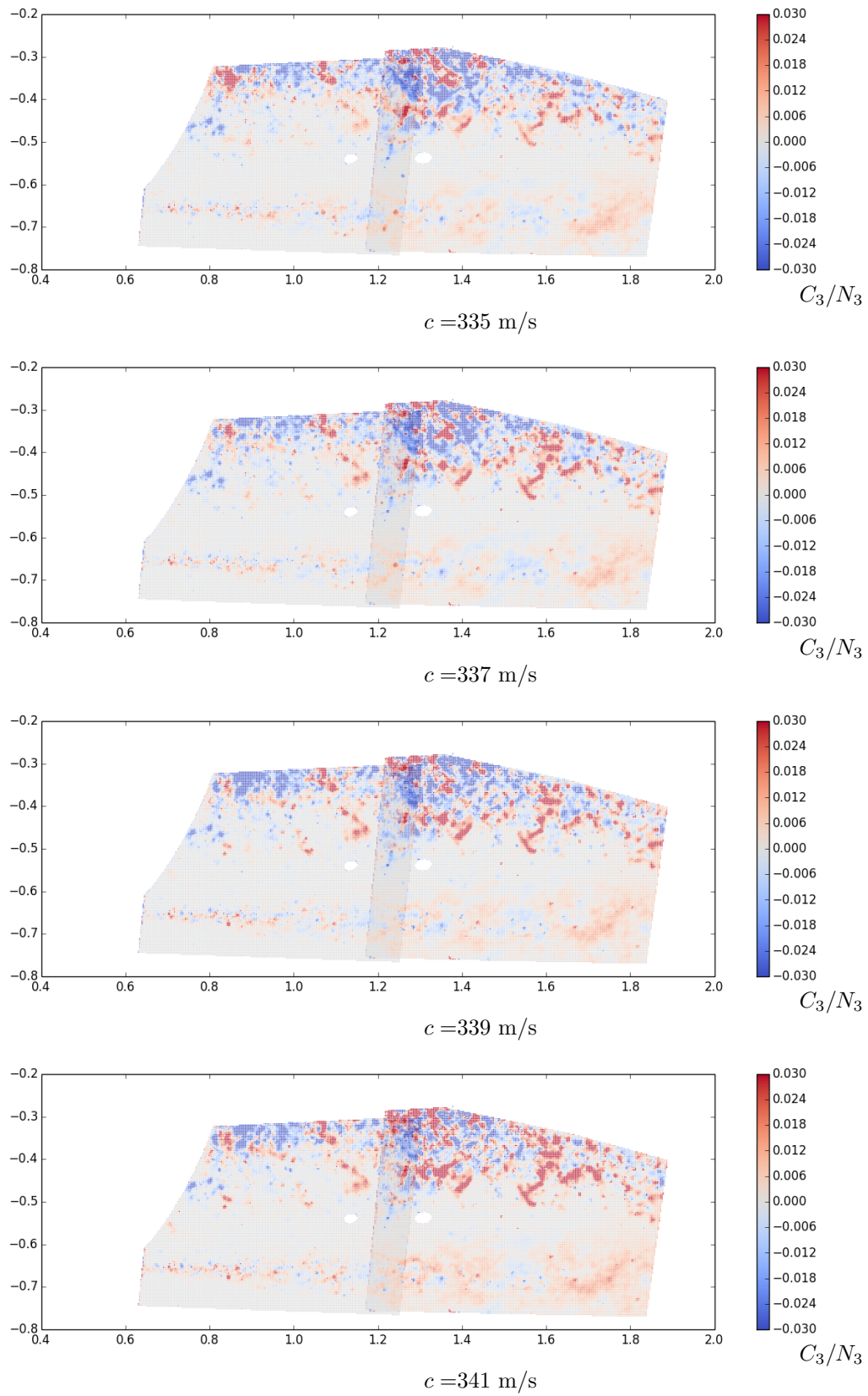


Figure 8. Normalized  $C_3$  for the test point 40, at varying speed of sound.

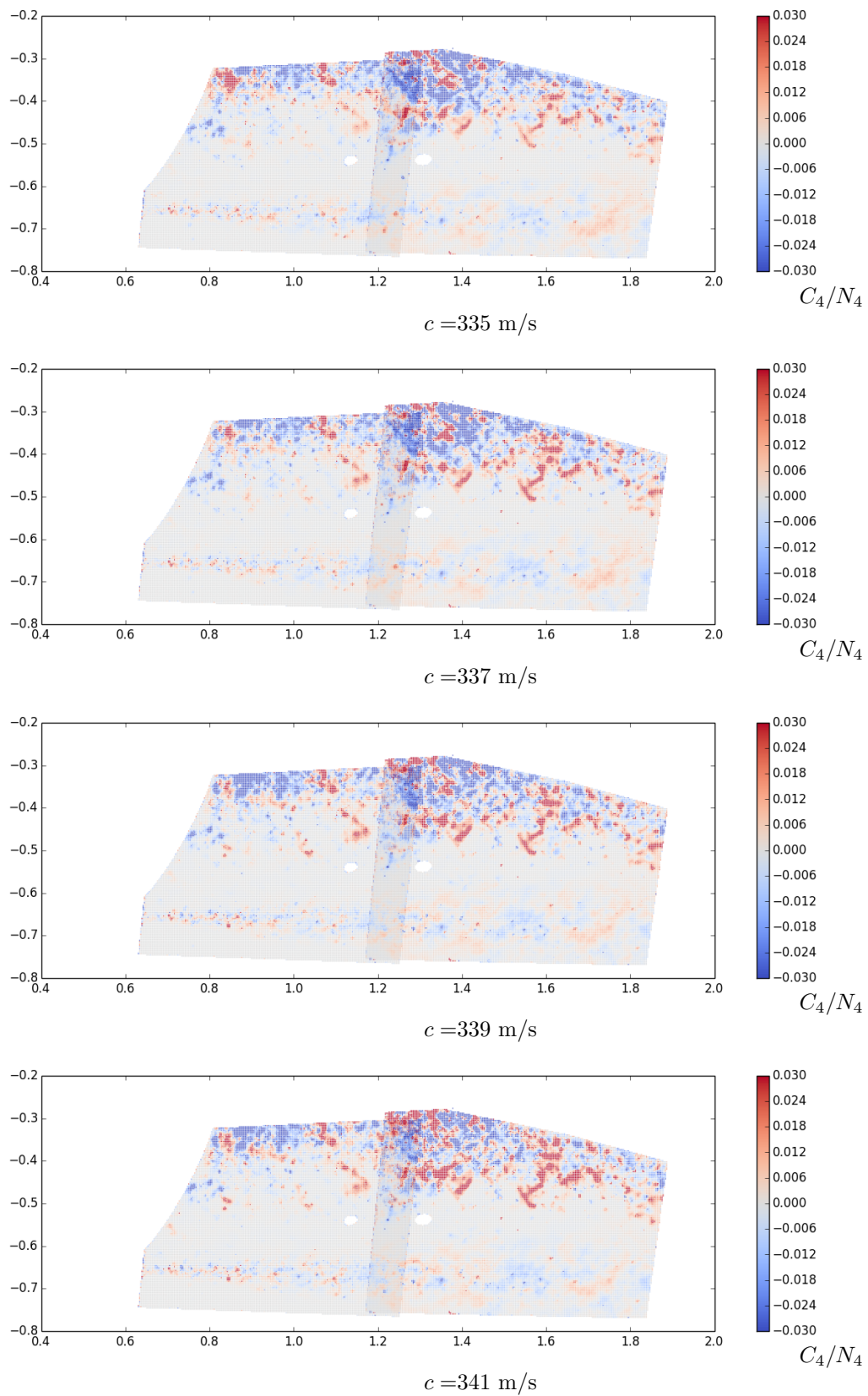


Figure 9. Normalized  $C_4$  for the test point 40, at varying speed of sound.

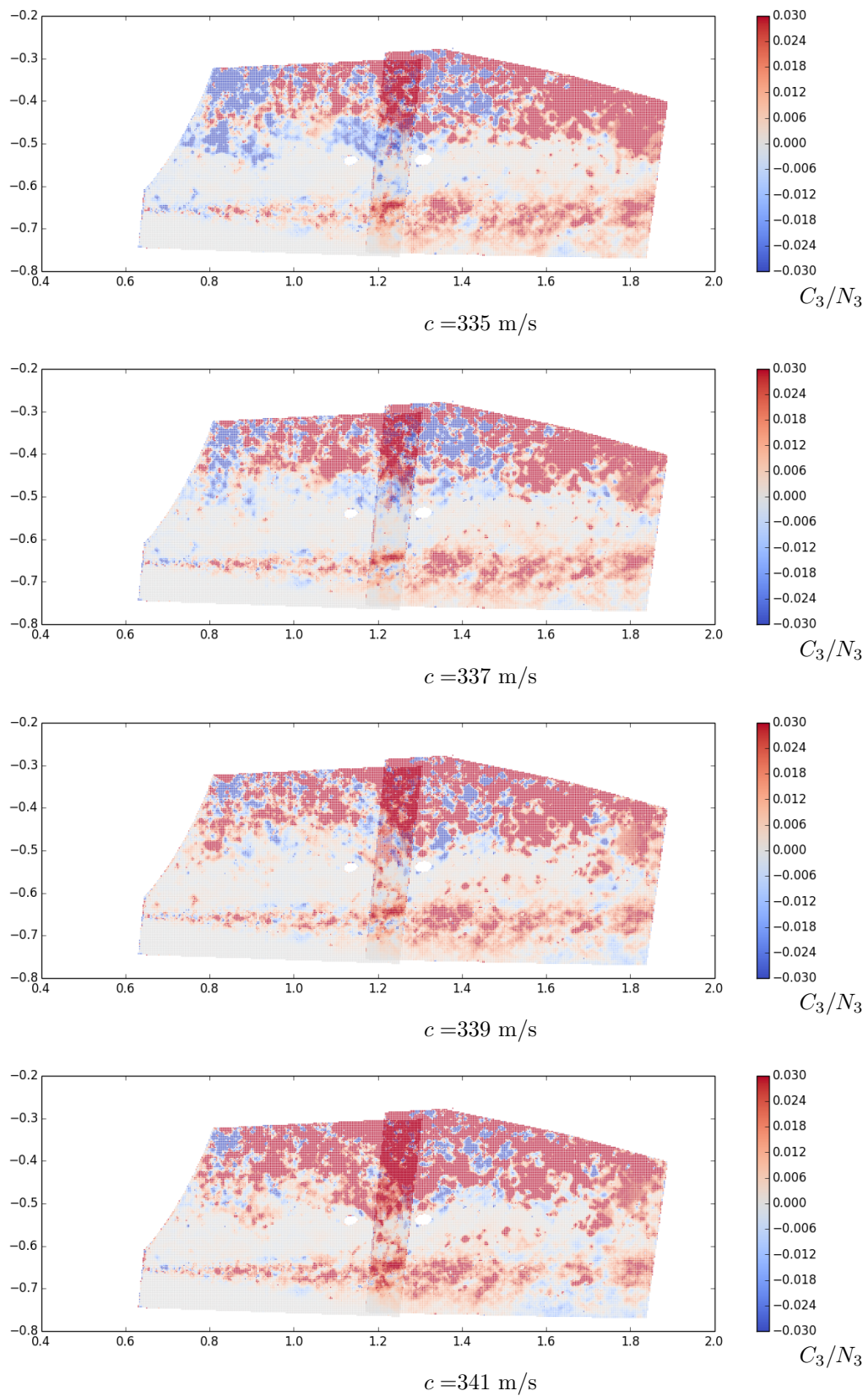


Figure 10. Normalized  $C_3$  for the test point 42, at varying speed of sound.

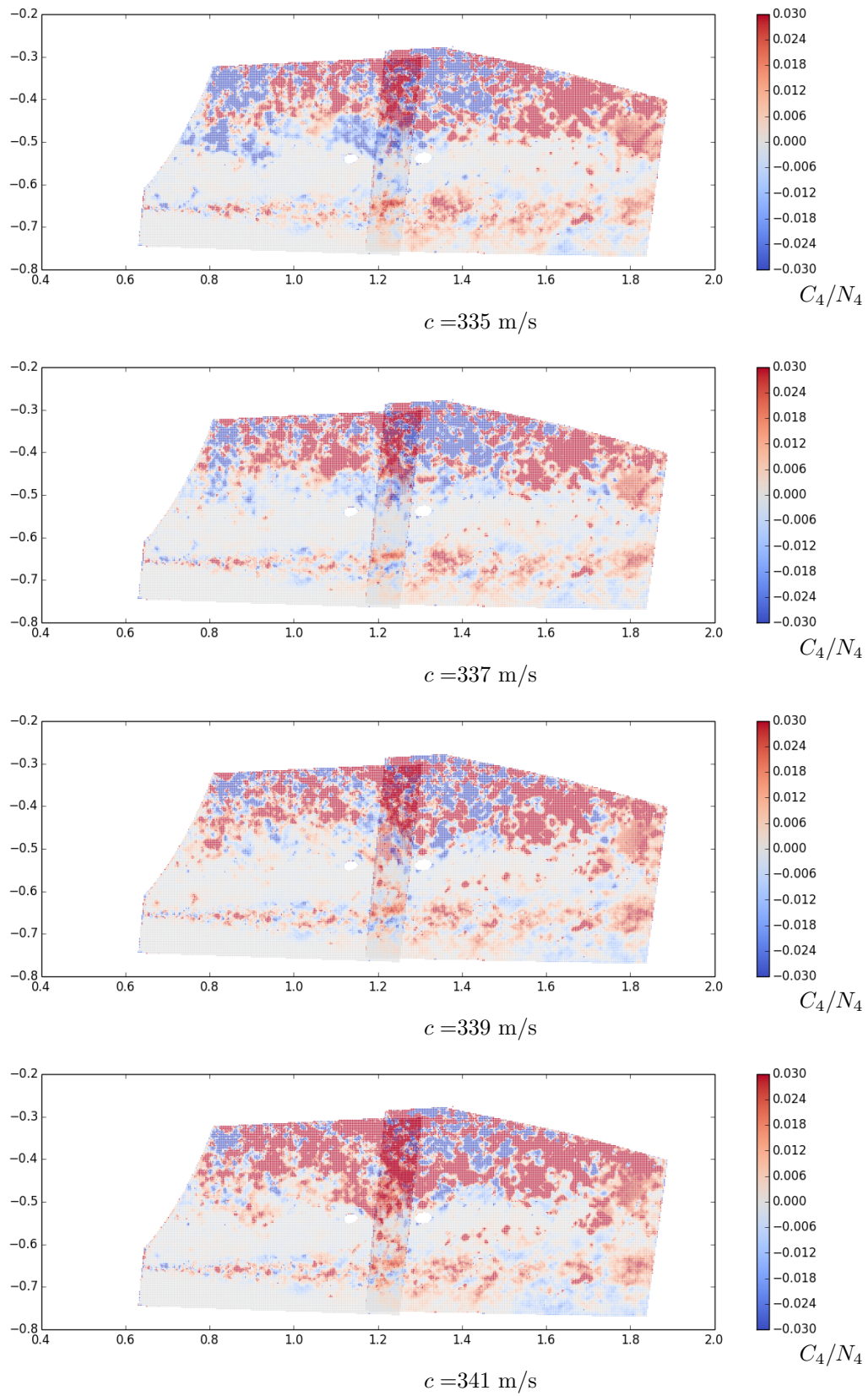


Figure 11. Normalized  $C_4$  for the test point 42, at varying speed of sound.